

# An optimized perfectly matched layer for the Schrödinger equation

Anna Nissen      Gunilla Kreiss

June 26, 2009

## Abstract

A perfectly matched layer (PML) for the Schrödinger equation using a modal ansatz is presented. We derive approximate error formulas for the modeling error from the outer boundary of the PML and for the error from the discretization and show how these can be matched in order to obtain optimal performance of the PML. Included numerical results show that the PML works efficiently at a prescribed accuracy for the zero potential case, with a layer of width less than two percent of the computational domain.

## 1 Introduction

Propagating waves are important in many fields of applications, such as electromagnetism, acoustics, aerodynamics and quantum mechanics. These types of problems are often formulated on very large or unbounded domains and an important aspect in performing efficient numerical simulations is to restrict the original domain to a much smaller computational domain. In order to mimic the behavior of outgoing waves on an unbounded domain, artificial boundary conditions need to be imposed on the boundary of the computational domain. An important feature of this boundary is that it should not reflect outgoing waves, that would contaminate the solution of the original problem. Such artificial boundary conditions can be divided into two classes: non-reflecting or absorbing boundary conditions (ABC) and absorbing layers. An ABC is posed precisely on the boundary, whereas an absorbing layer is an extension of the computational domain where outgoing waves are dampened. See e.g. Hagstrom [1], [2] and Givoli [3] for extensive reviews on ABC's.

Here, we consider solving the time-dependent Schrödinger equation with a member from the second class, a perfectly matched layer (PML), in order to study the behavior of quantum mechanical systems without having spurious reflections from waves traveling out of the domain. This is an important issue when studying the dynamics of a chemical reaction, e.g. when the quantum mechanical system consists of a molecule that dissociates into two smaller molecules. Here, the square of the absolute value of the wave function corresponds to a probability distribution. The independent variable is the distance between the subsystems. Hence, as the distance between the subsystems increases, a probability wave propagates towards the far-field.

The perfectly matched layer (PML) method was developed for Maxwell's equations by Berenger in 1994 [4] and has been successfully used in computational electromagnetics where it has become the standard method. The idea of the PML method is to surround the computational domain by an artificial damping layer of finite width, where a modified set of equations have to be solved. Ideally, the incoming waves are damped to such an extent that the outer boundary conditions are of no importance. Also, the interface between the computational domain and the damping layer should not cause any reflections. The PML fulfils this criteria in theory, although some reflections occur in practice due to the discretization of the problem. We will refer to these as numerical reflections.

The aim of this work is to show how to systematically choose damping parameters and discretization parameters for optimal performance of a Schrödinger PML. A related study for Maxwell's equations in second order formulation was done in [5]. We focus on spatial discretization by finite difference methods and consider orders 2 and 4. In time we use a finite difference scheme of order 2, but the study is also relevant for more efficient time propagation methods. In particular we have the Magnus-Arnoldi schemes [6] in mind.

In comparison with ABC's, relatively little work has been done on PMLs for the Schrödinger equation. However, the PML approach is closely related to absorbing boundary methods used in the quantum chemistry community, and our results can be extended to such methods.

The disposition of the article is as follows: in section 1.1 we give an overview of the relevant layers in the quantum chemistry community. In section 2 the modified PML equation is derived and the relation between smooth exterior scaling (SES) and PML is discussed. We consider numerical approximations in section 3. Error analysis is considered in section 4, where we derive approximate formulas for numerical errors and error caused by the finite width of the layer. Numerical experiments are performed in section 5, verifying the error formulas derived in section 4 and showing how these

yield optimal results. Conclusions and suggestions for future work are given in section 6.

## 1.1 Damping layers in the quantum chemical community

An important task of quantum chemistry is to be able to calculate the energy of resonance states. A resonance state is defined as a long-lived state of a system which has sufficient energy to break up into two or more subsystems [7]. In scattering experiments, the subsystems can for instance be an electron which is scattered from an atom or a molecule. The resonance states are discrete solutions of the Schrödinger equation with exponentially divergent wavefunctions at large distances from the scattering center and are thus not elements of a Hilbert space. There are different techniques to address this issue in computations. One technique is complex scaling, where a coordinate transformation,  $x \rightarrow F(x) = xe^{i\theta}$ , into the complex plane leads to square integrability of the resonance wave eigenfunctions, i.e. after the transformation the eigenfunctions belong to the Hilbert space, while the resonance energies remain unaffected [7]. Using complex scaling for molecular problems means that a potential energy surface (PES), which is given as a set of *ab initio* points, needs to be scaled and interpolated between the points by analytic functions. Smooth exterior scaling (SES) is based on the theory of complex scaling, but the coordinate transformation occurs after some  $x = x_0$ , after which the PES is assumed to be constant. Hence, by using the SES technique the scaling of the PES can be avoided. However, the most common approach in the quantum chemistry community is to add a complex absorbing potential (CAP) to the physical Hamiltonian right outside the domain of interest. The main reason that the CAP's are so popular is that they are easy to implement together with psuedo-spectral methods, a diagonal complex matrix is simply added to the Hamiltonian. However, the spectrum of the perturbed Hamiltonian will be affected for the CAP method, causing unphysical effects. A significant advantage for the SES and complex scaling over CAP is that they stand on a more rigorous mathematical ground [8].

## 2 The Schrödinger equation with PML

We modify the Schrödinger equation in the PML following Hagstrom [2]. Consider the time-dependent Schrödinger equation in two space dimensions

$$(1) \quad i \frac{\partial u}{\partial t} = -\frac{\partial^2 u}{\partial x^2} + L(y, \partial/\partial y)u \quad \text{in } \Omega = [0, \infty) \times [-l, l], \quad (1)$$

with boundary operators  $B_1$  and  $B_2$  in the  $y$ -direction

$$B_1 u(x, -l, t) = B_2 u(x, l, t) = 0,$$

and a decay condition

$$\lim_{x \rightarrow \infty} u(x, y, t) = 0. \quad (2)$$

Here  $L$  is a linear, elliptic operator

$$L(y, \partial/\partial y) = -\frac{\partial^2}{\partial y^2} + V(y),$$

with eigenvalues  $\kappa_j^2$  and eigenvectors  $\psi_j$

$$L\psi_j = \kappa_j^2 \psi_j \quad j = 1, \dots, \infty.$$

We want to truncate the infinite domain in the  $x$ -direction by constructing a PML of width  $d$  at  $x = x_0$ , so that the new domain is reduced to  $\Omega = [0, x_0 + d] \times [-l, l]$ . Expanding  $u$  in a Fourier series in the  $\psi_j$  and Laplace-transforming in time gives the equation

$$is\hat{u}_j = -\frac{\partial^2 \hat{u}_j}{\partial x^2} + \kappa_j^2 \hat{u}_j \quad \text{in } \Omega = [0, \infty) \times [-l, l],$$

with solutions

$$\hat{u}_j(x) = e^{\lambda_{\pm} x} \phi_j, \quad (3)$$

where  $\phi_j$  is a scalar and

$$\lambda_{\pm} = \pm \sqrt{-is + \kappa_j^2}.$$

We want to modify (3) so that solutions that propagate into the layer are damped. We consider  $Re(s) \geq 0$  and choose the branch of the square root so that

$$Re\left(\sqrt{-is + \kappa_j^2}\right) \leq 0 \quad \text{for } Re(s) \geq 0.$$

$\lambda_+$  gives bounded solutions that satisfy (2) and decaying waves can be obtained by modifying the exponent in the following way

$$\hat{u}_j(x) = e^{\sqrt{-is + \kappa_j^2}(x + e^{i\gamma} \int_{x_0}^x \sigma(\omega) d\omega)}, \quad (4)$$

where  $\sigma(\omega)$  is a smooth, non-negative function in  $\omega$ .  $\gamma$  is usually a constant grid stretching parameter chosen as  $0 < \gamma < \frac{\pi}{2}$  in order to obtain decaying solutions. An alternative is to let  $\gamma$  vary with  $x$  in the PML, i.e.  $\gamma = \gamma(x)$ . For perfect matching the solution and its derivative in the interior domain should coincide with the modified solution and its derivative in the layer at the interface  $x = x_0$ . Thus we need to impose the additional condition

$$\sigma(x_0) = 0.$$

Solutions of the form (4) are obtained by solving

$$i \frac{\partial u}{\partial t} = - \frac{1}{1 + e^{i\gamma}\sigma(x)} \frac{\partial}{\partial x} \frac{1}{1 + e^{i\gamma}\sigma(x)} \frac{\partial u}{\partial x} + L(y, \partial/\partial y)u \quad (5)$$

$$\text{in } \Omega = [0, x_0 + d] \times [-l, l]$$

instead of (1). Note that if  $\sigma(x) = 0$  for  $x \leq x_0$ , (5) reduces to (1) in the interior domain. Hence, we can solve (5) both in the interior domain and in the layer by letting  $\sigma(x)$  vanish in the interior.

Remark: The derivation generalizes to more space dimensions.

## 2.1 Relation between PML and smooth exterior scaling

The idea of smooth exterior scaling is the same as for the PML, that outgoing waves are dampened as they travel out of the computational domain by gradually increasing some absorption parameter towards the outer boundary. One way of viewing the PML method is as a complex coordinate stretch, where the real coordinate  $x$  is replaced by a complex coordinate  $F(x)$  in the layer. This was first done by Chew and Weedon [9], and in this setting it becomes clear that the PML and SES approaches are in fact equivalent, only written on different forms. Considering

$$F(x) = x + e^{i\gamma} \int_{x_0}^x \sigma(\omega) d\omega$$

as a continuation of the real coordinate  $x$  into the complex plane in the layer leads to equation (6)

$$i \frac{\partial u}{\partial t} = - \frac{\partial^2 u}{\partial F^2} + L(y, \partial/\partial y)u = - \frac{1}{f(x)} \frac{\partial}{\partial x} \frac{1}{f(x)} \frac{\partial u}{\partial x} + L(y, \partial/\partial y)u, \quad (6)$$

where

$$\frac{dF(x)}{dx} = f(x) = 1 + e^{i\gamma}\sigma(x),$$

and thus (6) is the same equation as (5). In SES the ansatz  $u(x, t) = k(x)\varphi(x, t)$  (6) is made, which for the new wave function  $\varphi(x, t)$  leads to the equation

$$i\frac{\partial\varphi}{\partial t} = -\frac{1}{f(x)}\frac{\partial^2}{\partial x^2}\frac{1}{f(x)}\varphi + V_k(x)\varphi + L(y, \partial/\partial y)\varphi, \quad (7)$$

with a complex symmetric operator on the right hand side. Here  $V_k(x) = (3f'(x)^2 - 2f''(x)f(x))/4f(x)^4$  and  $k(x)$  is chosen as  $k(x) = \frac{1}{\sqrt{f(x)}}$  in order to eliminate the first derivatives in  $\varphi(x)$  that appear from inserting the ansatz into (6). Using this complex symmetric expression (7) for the space discretization could be advantageous since theorems and proofs for hermitian matrices can be transferred to complex symmetric matrices by using a so called *c-product* [7]. Another reason is that it gives a larger basis of option when choosing methods for time-propagation. For example, Lanczos iteration for complex symmetric matrices could be used, although this method has been known to suffer from numerical instabilities [10].

### 3 Numerical approximations

We solve the Schrödinger equation using two finite difference schemes of Crank-Nicolson type, they are second order accurate in time and second and fourth order accurate in space, respectively. The second order method is

$$i\frac{u_j^{n+1} - u_j^n}{\Delta t} = \frac{v_j}{\Delta x^2} \left[ v_{j+1/2} \left( \frac{u_{j+1}^{n+1} + u_{j+1}^n}{2} - \frac{u_j^{n+1} + u_j^n}{2} \right) - v_{j-1/2} \left( \frac{u_j^{n+1} + u_j^n}{2} - \frac{u_{j-1}^{n+1} + u_{j-1}^n}{2} \right) \right], \quad (8)$$

$u_j^n$  is the grid function with space index  $j$  and time index  $n$ .  $v_{j+1/2}$  are calculated as mean values of the analytical function  $v(x)$  (9) between the two grid points  $j$  and  $j + 1$ , where

$$v(x) = \frac{1}{1 + e^{i\gamma\sigma(x)}}. \quad (9)$$

The Crank-Nicolson scheme without PML,

$$i\frac{u_j^{n+1} - u_j^n}{\Delta t} = \frac{1}{\Delta x^2} \left( \frac{u_{j+1}^{n+1} - 2u_j^{n+1} + u_{j-1}^{n+1}}{2} + \frac{u_{j+1}^n - 2u_j^n + u_{j-1}^n}{2} \right), \quad (10)$$

is unconditionally stable, hence the time step should only be restricted due to accuracy requirements. Energy estimates for the continuous PML equation with constant coefficients and Dirichlet or periodic boundary conditions yields the following restriction on  $\gamma$  for well-posedness,

$$0 < \gamma < \frac{\pi}{2}. \quad (11)$$

Hence, (8) will with that choice of  $\gamma$  be stable for any constant absorption function  $\sigma \geq 0$ . Numerical experiments suggest that the same is true also for the variable coefficient case.

Inserting an exact solution  $u(x, t)$  into the semi-discrete equation,

$$i \frac{\partial u_j}{\partial t} = -\frac{v_j}{\Delta x^2} [v_{j+1/2} (u_{j+1} - u_j) - v_{j-1/2} (u_j - u_{j-1})] \equiv D_2 u_j, \quad (12)$$

where  $u_j(t)$  is the numerical semi-discrete solution, yields a truncation error where the largest term

$$T_{\varepsilon_2} = -\Delta x^2 v \left( \frac{v u_{xxxx}}{12} + \frac{v_x u_{xxx}}{6} + \frac{v_{xx} u_{xx}}{8} + \frac{v_{xxx} u_x}{24} \right), \quad (13)$$

is of second order. The fourth order in space, second order in time-scheme (16) is obtained by first combining (9) and the right hand side of (5) and expanding, see (14), and then discretizing using central finite differences of fourth order, see (15).

$$-v(x) \frac{\partial}{\partial x} \left( v(x) \frac{\partial u}{\partial x} \right) = -v(x)^2 \frac{\partial^2 u}{\partial x^2} - v(x) \frac{\partial v}{\partial x} \frac{\partial u}{\partial x}, \quad (14)$$

$$i \frac{\partial u_j}{\partial t} = -\frac{v_j^2}{12 \Delta x^2} [-u_{j+2} + 16u_{j+1} - 30u_j + 16u_{j-1} - u_{j-2}] - \frac{v_j v_{x,j}}{12 \Delta x} [-u_{j+2} + 8u_{j+1} - 8u_{j-1} + u_{j-2}] \equiv D_4 u_j. \quad (15)$$

Here  $v_j$  and  $v_{x,j}$  are the exact function values of  $v(x)$  and  $v_x(x)$ , respectively, in grid point  $j$ . The fourth order in space, second order in time-scheme (16) is

$$i \frac{u_j^{n+1} - u_j^n}{\Delta t} = D_4 \left( \frac{u_j^{n+1} + u_j^n}{2} \right). \quad (16)$$

The stability properties of (8) and (16) are good. A drawback is that the Crank Nicolson method is an implicit method and a system of equations needs to be solved in each time step.

Remark: We can add terms to increase the order in space additionally, but since the scheme is only second order in time a higher order in space discretization will force us to take very small time steps to retain a high accuracy. However, this can be done if another method is used for time-propagation. It is also useful when expanding into higher dimensions in space.

## 4 Error analysis

There are three types of errors which affect the solution of the discretized problem on the truncated domain; the error that comes from solving the continuous Schrödinger equation on a truncated domain with a PML of finite width,  $\varepsilon_1$ , the error that comes from discretizing the modified equation (5) in the PML,  $\varepsilon_2$ , and the discretization error from the interior domain,  $\varepsilon_0$ .  $\varepsilon_1$  is referred to as the modeling error,  $\varepsilon_2$  as the numerical reflections and  $\varepsilon_0$  as the discretization error.

For optimal performance we want to match the modeling error,  $\varepsilon_1$ , with the numerical reflections,  $\varepsilon_2$ , so that neither of the errors dominate, but are of the same order. Moreover, the error level should be determined by the discretization error from the interior,  $\varepsilon_0$ , so that  $\varepsilon_1$  and  $\varepsilon_2$  are of the same order as  $\varepsilon_0$ .

### 4.1 Modeling error

In this section we consider  $\varepsilon_1$ .  $\varepsilon_2$  is considered in section 4.2 and  $\varepsilon_0$  in section 4.3. We start with the solutions to the Laplace-transformed versions of (1) and (5), respectively,

$$\hat{u}(x) = Ae^{-\sqrt{-is+\kappa_j^2}x} + Be^{\sqrt{-is+\kappa_j^2}x},$$

$$\hat{u}_{PML}(x) = A_{PML}e^{-\sqrt{-is+\kappa_j^2}(x+e^{i\gamma}\int_{x_0}^{x_0+d}\sigma(\omega)d\omega)} + B_{PML}e^{\sqrt{-is+\kappa_j^2}(x+e^{i\gamma}\int_{x_0}^{x_0+d}\sigma(\omega)d\omega)},$$

consisting of one wave propagating to the left and one propagating to the right. Imposing a Dirichlet boundary condition at the outer boundary of the layer,  $x = x_0 + d$ , gives

$$\hat{u}_{PML}(x_0 + d) = 0 \Rightarrow B_{PML} = -A_{PML}e^{-2\sqrt{-is+\kappa_j^2}(x_0+d+e^{i\gamma}\int_{x_0}^{x_0+d}\sigma(\omega)d\omega)}.$$

By matching solutions to (1) and (5) and their derivatives at  $x = x_0$ , an expression for the modeling error, the ratio between the incoming (left-propagating) and outgoing (right-propagating) wave in the interior domain,

can be derived.

$$\varepsilon_1 = \frac{|A_{PML}|}{|B_{PML}|} = e^{2\delta}, \quad \delta = \operatorname{Re} \left( \lambda_+ \left( x_0 + d + e^{i\gamma} \int_{x_0}^{x_0+d} \sigma(\omega) d\omega \right) \right), \quad (17)$$

$$\lambda_+ = \sqrt{-is + \kappa_j^2}.$$

We see that the modeling error depends on the width of the PML, the size of the integral of  $\sigma(x)$  and on the specific problem in terms of  $\kappa_j^2$  and  $s$ . However, it is independent of the shape of  $\sigma(x)$ .

In order to derive approximate expressions for the modeling error,  $\varepsilon_1$ , and later for the numerical reflections from the PML,  $\varepsilon_2$ , we need to determine the dominating frequencies of the incoming wavepacket. Consider the model problem (18) where  $L(y, \partial/\partial y)$  from (1) is zero:

$$i \frac{\partial u}{\partial t} = - \frac{\partial^2 u}{\partial x^2} \quad (18)$$

$$u(x, 0) = e^{-x^2 + ikx},$$

so that  $k$  is the speed of the incoming wave packet. Laplace-transformation in time gives

$$is\hat{u} = - \frac{\partial^2 \hat{u}}{\partial x^2} + ie^{-x^2 + ikx}.$$

Fourier-transformation in  $x$  gives

$$is\hat{\bar{u}} = -(i\omega)^2 \hat{\bar{u}} + i\sqrt{\pi} e^{-(\omega-k)^2/4},$$

and we get the Laplace- and Fourier-transformed solution  $\hat{\bar{u}}$

$$\hat{\bar{u}} = \frac{i\sqrt{\pi}}{is - \omega^2} e^{-(\omega-k)^2/4}, \quad (19)$$

where  $\hat{\bar{u}}$  is exponentially decaying and attains large values when  $\omega \approx k$ , and when  $is \approx \omega^2$ . Hence,  $s \approx k^2/i = -ik^2$  gives large values of  $\hat{\bar{u}}$ .

Remembering that  $\operatorname{Re}(s) \geq 0$ , we insert  $s = -ik^2 + \alpha_1$  into  $\lambda_+ = \sqrt{-is + \kappa_j^2}$  with  $\kappa_j = 0$  and  $\alpha_1 > 0$ ,  $\alpha_1 \ll k$ . Due to the choice of branch for the square root this yields

$$\lambda_+ = +\sqrt{-i(-ik^2 + \alpha_1)} = ik + \mathcal{O}\left(\frac{\alpha_1}{k}\right), \quad (20)$$

with  $\operatorname{Re}(\lambda_+) < 0$ . Using a polynomial of degree  $p$  as absorption function yields the integral

$$\int_{x_0}^{x_0+d} \sigma(\omega) d\omega = \int_{x_0}^{x_0+d} \sigma_{max} \left( \frac{\omega - x_0}{d} \right)^p = \left[ \sigma_{max} \frac{(\omega - x_0)^{p+1}}{(p+1)d^p} \right]_{x_0}^{x_0+d} = \sigma_{max} \frac{d}{p+1}. \quad (21)$$

Inserting (20) and (21) into (17) yields

$$\varepsilon_1 \approx e^{\frac{-2k \sin(\gamma) \sigma_{max} d}{p+1}}. \quad (22)$$

Here we used the approximation  $\lambda_+ \approx ik$ . The modeling error should according to (22) decrease exponentially as the wave number,  $k$ , the width of the PML,  $d$ , and the strength of the absorption,  $\sigma_{max}$ , increase. Note that by letting  $\sigma_{max}$  depend on the degree of the polynomial,  $p$ , the value of the integral can be kept constant independently of  $p$ . The expression (22) is validated numerically in section 5.

Consider a rightgoing wave,

$$\hat{u}(x) \approx e^{ik(x+e^{i\gamma} \int_{x_0}^x \sigma(\omega) d\omega)}. \quad (23)$$

With  $\lambda_+ = ik_2 - \alpha_2$ , we have

$$\hat{u}(x) \approx e^{(ik_2 - \alpha_2)(x + \Sigma_a + i\Sigma_b)} = e^{ik_2(x + \Sigma_a) - i\alpha_2 \Sigma_b} e^{-k_2 \Sigma_b - \alpha_2(x + \Sigma_a)}, \quad (24)$$

where  $e^{i\gamma} \int_{x_0}^x \sigma(\omega) d\omega = \Sigma_a + i\Sigma_b$ . Here  $\Sigma_a$  and  $\Sigma_b$  are real and positive.

Note that  $\Sigma_a$  corresponds to a real grid stretch, whereas  $\Sigma_b$  corresponds to a continuation of  $x$  into the complex plane. The Schrödinger equation is dispersive in nature and both  $\Sigma_a$  and  $\Sigma_b$  will contribute to the dampening of the wavepacket, although in general most of the dampening stems from  $\Sigma_b$ .

An alternative to the standard constant grid stretch parameter  $\gamma$  is to use  $\gamma = \gamma(x)$ . For instance, letting  $\gamma$  start near  $\pi/2$  and gradually decrease will gradually increase the real grid stretch in the PML, i.e. the discretization in the PML will be coarser further into the PML. Since the wavepacket is much smaller further into the PML, to gradually coarsening the grid in the PML would likely not contribute to an increase in the total error, even though the resolution there is decreased. Hence, less points can be used in the PML without losing accuracy. This is not investigated further here, instead a constant value of  $\gamma = \pi/4$  is used, if nothing else is stated.

## 4.2 Numerical reflections from the PML

Discretizing the continuous PML equation (5) introduces numerical reflections,  $\varepsilon_2$ , which depend on the truncation error inside the PML. The truncation error for the second order scheme (8) is

$$T_{\varepsilon_2} = -\Delta x^2 v \left( \frac{v u_{xxxx}}{12} + \frac{v_x u_{xxx}}{6} + \frac{v_{xx} u_{xx}}{8} + \frac{v_{xxx} u_x}{24} \right).$$

Inserting the semi-discrete, Laplace-transformed solution (23) together with (9) into the expression above yields an approximation of the truncation error

expressed in terms of  $\tilde{\sigma}(x) = e^{i\gamma}\sigma(x)$ , derivatives of  $\tilde{\sigma}(x)$ , wave number  $k$  and Laplace-transformed solution  $\hat{u}_j(x)$ ,

$$T_{\varepsilon_2,j} = -\Delta x^2 \frac{1}{1 + \tilde{\sigma}_j} \left[ -\frac{5}{24} k^2 \tilde{\sigma}_j'' + \frac{1}{24} \frac{1}{(1 + \tilde{\sigma}_j)} i k \tilde{\sigma}_j''' - \frac{1}{24} \frac{1}{(1 + \tilde{\sigma}_j)^2} i k \tilde{\sigma}_j' \tilde{\sigma}_j'' - \frac{1}{3} (1 + \tilde{\sigma}_j) i k^3 \tilde{\sigma}_j' + \frac{1}{12} (1 + \tilde{\sigma}_j)^3 k^4 \right] \hat{u}_j + \mathcal{O}(\Delta x^4). \quad (25)$$

Here, we have used the approximation  $\lambda_+ \approx ik$ . The discretization error in grid point  $j$ , i.e. the difference between an exact solution and a semi-discrete solution that fulfils (8) in that grid point, is denoted  $\varepsilon_{2,j}$  and fulfils

$$i \frac{\partial \varepsilon_{2,j}}{\partial t} = D_2 \varepsilon_{2,j} + T_{\varepsilon_2,j}, \quad (26)$$

i.e. the truncation error is transported with the error equation (26). Evaluation of the terms in (25) shows that the fourth term on the right hand side is the largest in the PML, indicating that the numerical reflections in the PML behave like

$$T_{\varepsilon_2,j} \propto \tilde{\sigma}' \Delta x^2 \hat{u}_j, \quad (27)$$

or by letting  $\sigma(x)$  be a polynomial of degree  $p$  according to (21),

$$T_{\varepsilon_2,j} \propto \frac{\sigma_{max}}{d^p} \Delta x^2 \hat{u}_j. \quad (28)$$

From (28) we expect the  $l_2$ -norm of the numerical reflections to behave like

$$\varepsilon_2 = C_2(k) \frac{\sigma_{max}}{d^p} \Delta x^2. \quad (29)$$

The behavior of the expression (29) with respect to  $\sigma_{max}$ ,  $d$ ,  $p$  and  $\Delta x$  is verified by numerical experiments in section 5. In section 5 we also see that  $\varepsilon_2$  decreases with increasing  $k$ .

### 4.3 Discretization error from the interior

For the scheme in the interior, where  $\tilde{\sigma} = 0$ , all terms but the fourth one in (25) will vanish, and the truncation error in the interior is approximately

$$T_{\varepsilon_0,j} \approx -\frac{\Delta x^2 k^4}{12} \hat{u}_j. \quad (30)$$

For a plane wave with spatial frequency  $k$ , the pointwise error in the interior at time  $T$ ,  $\varepsilon_{0,j} = |u(x_j, T) - u_j(T)|$ , is for the second order scheme at most

$$\max_j \varepsilon_{0,j} = \frac{\Delta x^2 k^4}{12} T + \mathcal{O}(\Delta x^4), \quad (31)$$

see [11], p.93.

Since the solution to the model problem (18) consists of many different frequencies, we cannot use this error bound in a strict sense here. However, we expect the  $l_2$ -norm of the discretization error from the interior domain to behave like

$$\varepsilon_0 \approx C \frac{\Delta x^2 k^4}{12} T. \quad (32)$$

Numerical tests presented in section 5 show that (32) gives a good estimation of the  $l_2$ -norm of the discretization error from the interior and that the proportionality constant  $C \approx 1$ . This is not surprising since the  $l_2$ -norm of the solution is of order unity.

#### 4.4 Matching of errors

Making the requirement that the numerical reflections,  $\varepsilon_2$ , should not amount to more than ten percent the discretization error from the interior,  $\varepsilon_0$ , yields

$$C_2(k) \frac{\sigma_{max}}{d^p} \Delta x^2 \leq 0.1 C_0(k, T) \Delta x^2.$$

We define  $M$  as

$$M = \frac{\sigma_{max}}{d^p}, \quad (33)$$

which gives

$$C_2(k) M \Delta x^2 \leq 0.1 C_0(k, T) \Delta x^2. \quad (34)$$

The constants  $C_2(k)$  and  $C_0(k, T)$  can be determined numerically and we get the largest possible value of  $M$  from (34)

$$M = \frac{0.1 C_0(k, T)}{C_2(k)}. \quad (35)$$

At the same time, we require that the modeling error from the PML,  $\varepsilon_1$ , should not exceed ten percent of  $\varepsilon_0$ , i.e.

$$e^{\frac{-2k \sin(\gamma) \sigma_{max} d}{p+1}} \leq 0.1 C_0(k, T) \Delta x^2.$$

Inserting (33) yields

$$\frac{-2k \sin(\gamma) M d^{p+1}}{p+1} \leq \ln(0.1 C_0(k, T) \Delta x^2), \quad (36)$$

and the smallest possible value of  $d$  can be determined from (36) as

$$d = \sqrt[p+1]{\frac{-\ln(0.1C_0(k, T)\Delta x^2)(p+1)}{2k \sin(\gamma)M}}. \quad (37)$$

Finally, the corresponding  $\sigma_{max}$  is determined from (33),

$$\sigma_{max} = Md^p. \quad (38)$$

## 5 Numerical experiments

Numerical experiments for the zero potential case are performed in 1D and we verify that the behavior of the modeling error agrees with theory. We show that the discretization error from the interior goes to zero at the expected rate as the mesh is refined for the second and fourth order in space schemes, (8) and (16). Also, we investigate how the numerical reflections from the PML depend on the PML parameters and how to choose PML parameters so that the different types of errors are matched. An interesting observation is that when the PML is sufficiently wide and the absorption function is smooth, the numerical reflections from the PML is often the least significant error as the wave packet is sufficiently resolved. For those grids, coarser grids actually perform slightly better, which likely is due to that finer grids succeed in transporting the error more efficiently.

We solve the model problem (18), which has the exact solution

$$u_{exact}(x, t) = \sqrt{\frac{i}{-4t+i}} e^{\frac{-ix^2-kx+kt^2}{-4t+i}}.$$

The numerical solution  $u_{PML}$  is compared to the exact solution,  $u_{exact}$ , and to a reference solution,  $u_{ref}$ , calculated on the same grid as  $u_{PML}$  but without PML and on a larger domain, so that the discretization error from the PML can be distinguished from the discretization error of the interior scheme. The  $l_2$ -error with respect to the exact solution is calculated at time  $T$  as

$$\frac{\|u_{PML}(\cdot, T) - u_{exact}(\cdot, T)\|_2}{\|u_{exact}(\cdot, 0)\|_2},$$

where  $\|u(\cdot, t)\|_2 = \sqrt{\Delta x \sum_i |u(x_i, t)|^2}$ . The sums are taken only over points in the interior domain. As absorption functions we use polynomials of degree  $p$ , on the form  $\sigma(x) = \sigma_{max} \left(\frac{x-x_0}{d}\right)^p$ , with  $p \geq 4$ .

## 5.1 Modeling error

We expect the modeling error,  $\varepsilon_1$ , to decrease exponentially with respect to wave number  $k$ , the strength of the absorption function  $\sigma_{max}$ , and the width of the PML  $d$ , see (22). Using (8) with  $\Delta x = 1 \cdot 10^{-3}$ ,  $\Delta t = 1 \cdot 10^{-4}$  on the domain  $x = [-5, 7]$ , where the PML starts at  $x_0 = 5$ , this behavior is verified and displayed in figure 1. We also see from figure 1 and tables 1 - 3 that the calculated modeling error agrees with the measured. An eighth order polynomial is used as absorption function with relatively low values of  $\sigma_{max}$  to ensure that the numerical reflections are small and the modeling error dominating.  $\sigma_{max}$ ,  $k$  and  $d$  are varied as stated in tables 1 - 3, elsewhere we have  $\sigma_{max} = 1.5$ ,  $k = 10$ ,  $d = 2$  and  $\gamma = \pi/4$ .

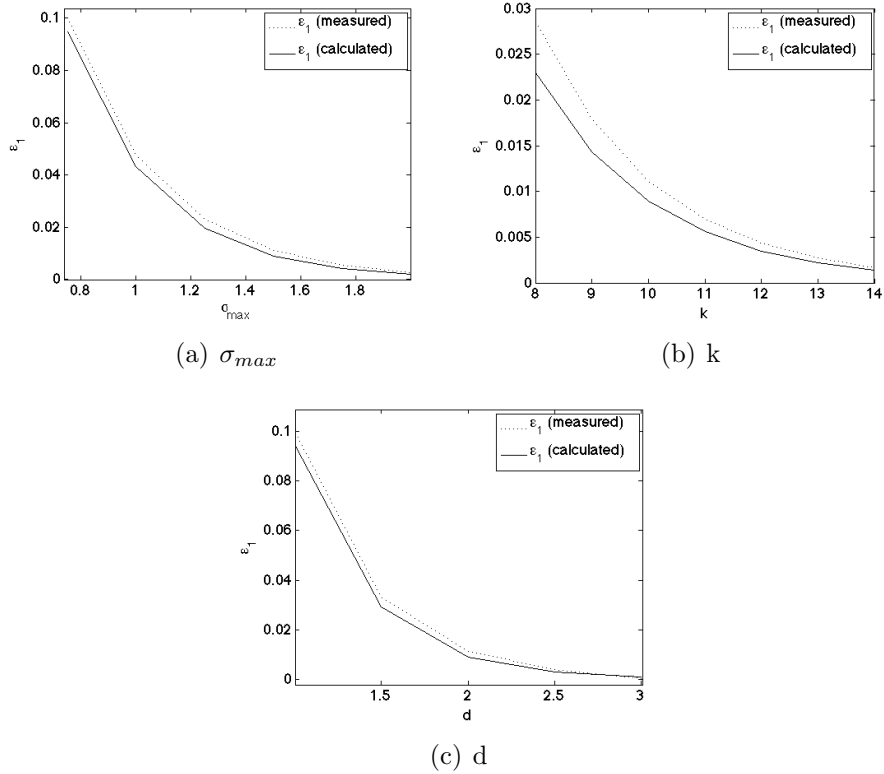


Figure 1: Modeling error as a function of  $\sigma_{max}$ ,  $k$  and  $d$

$\sigma_{max}$	$\varepsilon_1$ (measured)	$\varepsilon_1$ (predicted)
0.75	1.0011e-01	9.4702e-02
1	4.7645e-02	4.3166e-02
1.25	2.2957e-02	1.9676e-02
1.5	1.1120e-02	8.9682e-03
1.75	5.5310e-03	4.0879e-03
2	2.7657e-03	1.8633e-03

Table 1: Modeling error with varying  $\sigma_{max}$

$k$	$\varepsilon_1$ (measured)	$\varepsilon_1$ (predicted)
8	2.8572e-02	2.3024e-02
9	1.7938e-02	1.4370e-02
10	1.1120e-02	8.9682e-03
11	6.9895e-03	5.5974e-03
12	4.3621e-03	3.4935e-03
13	2.7224e-03	2.1804e-03
14	1.6990e-03	1.3608e-03

Table 2: Modeling error with varying  $k$

$d$	$\varepsilon_1$ (measured)	$\varepsilon_1$ (predicted)
1	1.0011e-01	9.4702e-02
1.5	3.3021e-02	2.9143e-02
2	1.11199e-02	8.9682e-03
2.5	3.9046e-03	2.7599e-03
3	1.3972e-04	8.4933e-04

Table 3: Modeling error with varying  $d$

We conclude that the behavior of the modeling error is in agreement with the theory in section 4.1 and that (22) gives a good estimate of the modeling error.

## 5.2 Numerical reflections

We expect the numerical reflections from the PML to depend on the step size  $\Delta x$ , the wave number  $k$ , the maximum value of  $\sigma(x)$ ,  $\sigma_{max}$ , as well as the shape of  $\sigma(x)$ . It should also depend on the width of the PML,  $d$ , as  $d^{-p}$ , where  $p$  is the order of the polynomial used. The discretization error

from the PML is transported to the interior domain, but also damped on the way by the PML. We expect the truncation error in the PML for the second order scheme to behave like

$$T_{\varepsilon_2, j} \propto \frac{\sigma_{max}}{d^p} \Delta x^2 \hat{u}_j.$$

The numerical reflections from the PML come from reflections from the interface as the wave packet propagates into the PML, as well as reflections inside the PML, that come from increasing the absorption function. For a constant shape of the absorption function, we investigate the behavior of the numerical reflections with respect to  $\Delta x$  and  $\sigma_{max}$ . We use a wide PML with  $d = 4$  to ensure that the modeling error is kept small and the numerical reflections from the interface of the PML is dominating.

We vary the grid size of the discretization as well as  $\sigma_{max}$  to investigate the behavior of the numerical reflections from the PML using (8). First, we keep the grid fixed with  $\Delta x = 3.2 \cdot 10^{-2}$  and we use  $\Delta t = 10^{-4}$  and a 4th order polynomial. Other constants are  $k = 10$ ,  $d = 4$ ,  $\gamma = \pi/4$ . In table 4 and 5 we see how the numerical reflections vary with  $\sigma_{max}$  and  $\Delta x$ , respectively. The linear and quadratic behaviors, respectively, are displayed in figure 2.

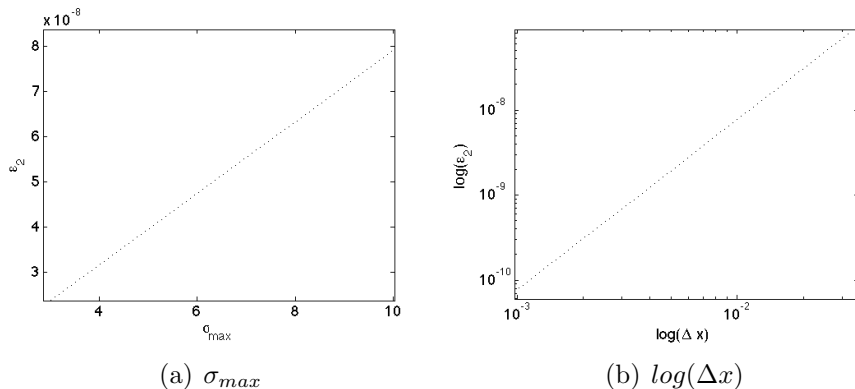


Figure 2: Numerical reflections  $\varepsilon_2$  as a function of  $\sigma_{max}$  and  $\log(\Delta x)$

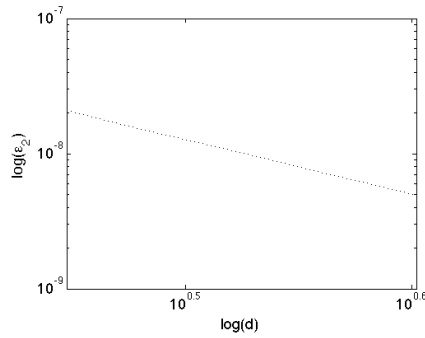
$\sigma_{max}$	$\varepsilon_2$ (measured)
3	2.3724e-08
4	3.1632e-08
5	3.9538e-08
6	4.7444e-08
7	5.5350e-08
8	6.3255e-08
9	7.1160e-08
10	7.9065e-08

Table 4: Numerical reflections with varying  $\sigma_{max}$

$\Delta x$	$\varepsilon_2$ (measured)	$\varepsilon_0$ (measured)	$\varepsilon_0$ (predicted)
3.2e-02	7.9065e-08	1.8241e-01	1.7237e-01
1.6e-02	1.9766e-08	4.5532e-02	4.3093e-02
8e-03	4.9414e-09	1.1510e-02	1.0773e-02
4e-03	1.2353e-09	3.0251e-03	2.6933e-03
2e-03	3.0876e-10	9.0634e-04	6.7333e-04
1e-03	7.7281e-11	3.7771e-04	1.6833e-04

Table 5: Numerical reflections with varying  $\Delta x$

In figure 3 and table 6, we see how  $\varepsilon_2$  depends of the width,  $d$ . Here we use  $\Delta x = 8 \cdot 10^{-3}$ ,  $\Delta t = 10^{-4}$ ,  $\sigma_{max} = 10$ ,  $p = 4$  and vary  $d$ . The slope in figure 3 is determined to  $-4.02$ , clearly showing a  $d^{-p}$ -behavior as expected.



(a)

Figure 3: Numerical reflections as a function of  $\log(d)$

$d$	$\varepsilon_2$ (measured)
2.8	2.0798e-08
3.0	1.5635e-08
3.2	1.2056e-08
3.4	9.4626e-09
3.6	7.5306e-09
3.8	6.0665e-09
4.0	4.9414e-09

Table 6: Numerical reflections with varying  $d$

In table 7,  $\Delta x = 8 \cdot 10^{-3}$  is kept and  $k$  is varied. We have  $d = 4$ ,  $\sigma_{max} = 10$ ,  $\Delta t = 10^{-4}$  and  $\gamma = \pi/4$ . The numerical reflections from the interface decrease as  $k$  increases, which is not what we would expect by looking at the truncation error (13). However, as we have seen the performance of the PML increases vastly for higher frequencies and this is likely an effect of that. For comparison we have included values of the interior discretization error obtained from (32) and by direct measurement from numerical experiments in the same table. We see that the measured interior discretization errors agree with the predicted values.

$k$	$\varepsilon_2$ (measured)	$\varepsilon_0$ (measured)	$\varepsilon_0$ (predicted)
8	7.9900e-09	5.9853e-03	5.3084e-03
9	6.1823e-09	8.4365e-03	7.6982e-03
10	4.9414e-09	1.1510e-02	1.0773e-02
11	4.0448e-09	1.5281e-02	1.4523e-02
12	3.3745e-09	1.9828e-02	1.9021e-02
13	2.8596e-09	2.5232e-02	2.4372e-02
14	2.4550e-09	3.1581e-02	3.0732e-02

Table 7: Discretization error with varying  $k$

In figure 4 we see the  $l_2$ -error in the interior as a function of time, for (8) in (a) and (b) and for (16) in (c) and (d), where (b) and (d) are close ups displaying parts of (a) and (c), respectively. The wave enters the PML shortly before  $t = 0.2$  and after  $t = 0.7$  the modeling error appears. We see in (a) that the modeling error for the finest discretization is of the same size as the modeling error for all discretizations in (c), but for coarser grids this error is smaller. This is likely due to that for coarser grids information is lost when the wave propagates. Here we have used parameter values  $k = 10$ ,  $p = 8$ ,  $\sigma_{max} = 9/4$ ,  $\gamma = \pi/4$ ,  $\Delta x = 1 \cdot 10^{-2}, 2 \cdot 10^{-2}, 4 \cdot 10^{-2}$  and  $\Delta t = 10^{-5}$ .

The numerical reflections from the interface is converging to zero for the 2nd order discretization, while the numerical reflections for the 4th order discretization is already on the order of roundoff, as we see in figures 4. The error from the interior scheme (where  $\sigma(x) = 0$ ) converges with 2nd and 4th order respectively, see figure 5.

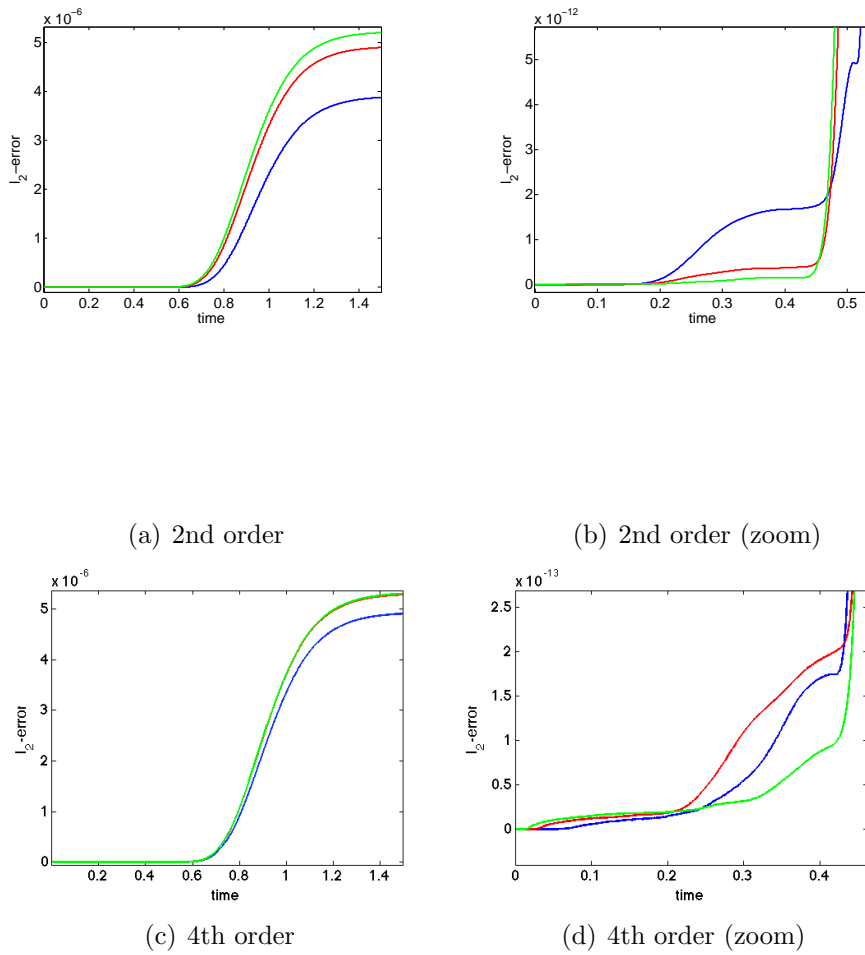


Figure 4:  $l_2$ -error as a function of time

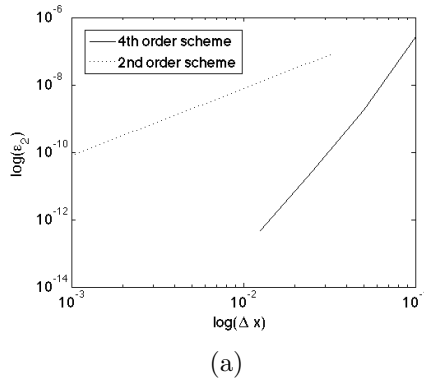


Figure 5: grid convergence of 2nd and 4th order schemes

Worth to note is that for well resolved wave packets the discretization error from the interior is dominating compared to the numerical reflections from the interface of the PML.

### 5.3 Matching of errors

We want to match the errors so that they are of the same order, where the magnitude is determined from the magnitude of the discretization error from the interior scheme,  $\varepsilon_0$ . Increasing  $\sigma_{max}$  makes the modeling error decrease, while the numerical reflections increase. An alternative way of decreasing the modeling error is to increase  $d$ , and this also decreases the numerical reflections from the PML. We match  $d$  and  $\sigma_{max}$  following the procedure described in section 4.4, so that a minimal number of points can be used in the PML for a given wanted accuracy.

We measure the discretization error from the interior and use it as error level.  $C_2(k)$  is determined to be  $C_2(10) \approx 4.9 \cdot 10^{-4}$  for  $p = 4$ . We continue by determining  $M$  from (35),  $d$  from (37) and  $\sigma_{max}$  from (38). The results from using the optimized values are displayed in table 8.

When we cannot choose the exact width due to the grid size, we choose to use one extra gridpoint. This gives much better result. The total measured error from the PML, denoted  $\varepsilon_m$ , and the relation between  $\varepsilon_m$  and  $\varepsilon_0$  is also presented in table 8. We have prescribed that the total error from the PML should be 20 percent or less, and we see that we get a slightly larger error from the PML than that. However, it never exceeds 30 percent of the interior error. Also, note that the width can be kept almost constant and the error is still reduced by increasing  $\sigma_{max}$ . The width  $d$  here amounts to less than 2 percent of the total domain.

$\Delta x$	$\varepsilon_0$ (measured)	$d$	$\sigma_{max}$	$\varepsilon_m$ (measured)	$\% \varepsilon_0$
3.2e-02	1.8246e-01	0.192	12.25	2.3910e-2	13.10
1.6e-02	4.5533e-02	0.192	12.23	8.7667e-3	19.27
8e-03	1.1509e-02	0.192	12.37	3.2230e-03	28.00
4e-03	3.0248e-03	0.196	14.12	8.7576e-04	28.95
2e-03	9.0628e-04	0.196	16.92	2.0179e-04	22.27
1e-03	3.7770e-04	0.180	20.07	1.0079e-04	26.69

Table 8: Matching errors with varying  $\Delta x$

## 6 Conclusions and future work

Our approximate error formulas describe qualitative behavior of the error with respect to strength of damping, thickness of the layer and grid size, which enables optimization of the PML. Numerical experiments show that by using our formulas it is possible to match the numerical reflections and the modeling error of the PML, so that the layer performs with a prescribed accuracy, as seen in table 8. Lowering the error tolerance calls for increased strength in the absorption parameter, but the width of the layer can be kept the same, here constituting of less than 2 percent of the computational domain. In the future, we plan to investigate the performance of our optimized PML in 2D and also for more realistic problems. We plan to expand the error analysis of the discretization error in the PML to higher order finite difference schemes, since higher order schemes are necessary in order to be able to tackle more realistic problems in quantum chemistry.

## References

- [1] T. Hagstrom, Radiation boundary condition for the numerical simulation of waves, *Acta Numerica* (1999) pp. 47-106.
- [2] T. Hagstrom, New results on absorbing layers and radiation boundary conditions, in: Ch.T. Hagstrom *Topics in Computational Wave Propagation*, in: M. Ainsworth, P. Davies, D. Duncan, P. Martin, B. Rynne (Eds.), *Lecture Notes in Computational Science and Engineering*, vol. 31, Springer-Verlag, New York, 2003, pp. 1-42.
- [3] D. Givoli, Non-reflecting boundary conditions, *J. Comput. Phys.* 94 (1991) 1-29.

- [4] J.P. Berenger, A perfectly matched layer for the absorption of electromagnetic waves, *J. Comput. Phys.* 114 (1994) 185-200.
- [5] B. Sjögreen, N.A. Petersson, Perfectly matched layers for Maxwell's equations in second order formulation, *J. Comput. Phys.* 209 (2005) 19-46.
- [6] K. Kormann, S. Holmgren, HO. Karlsson, Accurate time propagation for the Schrödinger equation with an explicitly time-dependent Hamiltonian, *J. Chem Phys.* 128 (2008) 184101-184101-11.
- [7] N. Moiseyev, Quantum theory of resonances: calculating energies, widths and cross-sections by complex scaling, *Physics report* 302 (1998) 211-293.
- [8] HO. Karlsson, Accurate resonances and effective absorption of flux using smooth exterior scaling, *J. Chem. Phys.* 109 (1998) 9366-9371.
- [9] W. C. Chew, W. H. Weedon, A 3-D perfectly matched medium from modified Maxwell's equations with stretched coordinates, *Micro. Opt. Tech. Lett.* 7 (1994) 599-604.
- [10] T. Sommerfeld, F. Tarantelli, Subspace iteration techniques for the calculation of resonances using complex symmetric Hamiltonians, *J. Chem. Phys.* 112 (1999) 2106-2110.
- [11] B. Gustafsson, H-O. Kreiss, J. Olinger, *Time-dependent problems and difference methods*, John Wiley & Sons, Inc. (1995).